DT-MRI Segmentation Using Graph Cuts

Yonas T. Weldeselassie and Ghassan Hamarneh

Medical Image Analysis Lab, School of Computing Science
Simon Fraser University, Burnaby, BC V5A 1S6, Canada

ABSTRACT

An important problem in medical image analysis is the segmentation of anatomical regions of interest. Once regions of interest are segmented, one can extract shape, appearance, and structural features that can be analyzed for disease diagnosis or treatment evaluation. Diffusion tensor magnetic resonance imaging (DT-MRI) is a relatively new medical imaging modality that captures unique water diffusion properties and fiber orientation information of the imaged tissues. In this paper, we extend the interactive multidimensional graph cuts segmentation technique to operate on DT-MRI data by utilizing latest advances in tensor calculus and diffusion tensor dissimilarity metrics. The user interactively selects certain tensors as object ("*obj*") or background ("*bkg*") to provide hard constraints for the segmentation. Additional soft constraints incorporate information about both regional tissue diffusion as well as boundaries between tissues of different diffusion properties. Graph cuts are used to find globally optimal segmentation of the underlying 3D DT-MR image among all segmentations satisfying the constraints. We develop a graph structure from the underlying DT-MR image with the tensor voxels corresponding to the graph vertices and with graph edge weights computed using either Log-Euclidean or the J-divergence tensor dissimilarity metric. The topology of our segmentation is unrestricted and both *obj* and *bkg* segments may consist of several isolated parts. We test our method on synthetic DT data and apply it to real 2D and 3D MRI, providing segmentations of the corpus callosum in the brain and the ventricles of the heart.

Keywords: Segmentation, diffusion tensor magnetic resonance imaging, graph cuts, tensor dissimilarity metric, Log-Euclidean, J-divergence

1. INTRODUCTION

Since Basser et al.[1] presented their seminal work on diffusion tensor magnetic resonance imaging (DT-MRI), the processing, analysis and visualization of this modality has become a primary focus in medical imaging research. As of today, it is the only non-invasive method that allows distinguishing the anatomical structures of the cerebral white matter by measuring local water diffusion through biological tissues. The result is an image where at each voxel, the direction of water diffusion is locally modeled by a Gaussian probability density function whose covariance matrix is a 3×3 symmetric positive definite diffusion tensor.

Image segmentation where regions of interest are delineated is necessary for performing subsequent quantitative analysis and qualitative visualization. In medical imaging applications, it is apparent that good quality segmentation helps radiologists extract shape, appearance, and other structural features that can be analyzed for disease diagnosis or treatment evaluation. Analogous to scalar image segmentation, DT-MR image segmentation can rely on (a) identifying nearby tensors with similar diffusion properties and grouping them into one coherent structure, (b) identifying edges in the images and linking them to form separating boundaries between neighboring structures, and (c) incorporating prior knowledge about shape characteristics of the different targets to segment.

While scalar image segmentation has been studied extensively and different algorithms have been developed over a long period of time, DT-MR image segmentation is a relatively new and challenging task. Zhukov et al.[2] proposed a level-set segmentation method that operates on a scalar field derived from the anisotropic diffusion tensors. However this method will fail to distinguish between regions of the same diffusion anisotropy magnitude but oriented in different directions. By incorporating the directions of diffusion in addition to the magnitude

{Y.T.W., G.H.}: E-mail: {yonas, hamarneh}@cs.sfu.ca, http://mial.cs.sfu.ca, Telephone: +1 604 291 5509

Medical Imaging 2007: Image Processing, edited by Josien P. W. Pluim, Joseph M. Reinhardt,
Proc. of SPIE Vol. 6512, 65121K, (2007) · 1605-7422/07/$18 · doi: 10.1117/12.710434

during segmentation process, one can differentiate between regions of same anisotropic diffusion but oriented in different directions. We show such an example using synthetic data in the results section (figure 2).

In order to improve the segmentation of DT-MRI data, one has to exploit all the information captured by the tensors. Zhizhou and Vemuri recently proposed a level-set based curve evolution technique for DT-MRI segmentation that operates on the diffusion tensor fields.[3] However, these variational formulations with iterative gradient descent based solutions are sensitive to parameter settings and initialization, and hence may get stuck at suboptimal local minima of the energy functional. Further, implementing intuitive user interaction remains a challenging goal in level set based segmentation techniques. On the other hand, interactive and highly-automated segmentation techniques keep the user 'in the loop' in an attempt to bridge the gap between the clinical users' expert knowledge and the inner workings of the computational tools and algorithms. Other DT-MRI segmentation techniques were proposed in the past few years.[4–12]

In this work, we extend the intuitive, interactive and globally optimal graph cuts scalar field segmentation technique proposed by Boykov and Jolly[13] to DT-MRI data. In our extension, the graph vertices correspond to the tensor voxels in the DT-MR image and the graph connectivity edge weights are computed using recently proposed mathematical frameworks of tensor dissimilarity metrics. Two such metrics are utilized in our work: the Log-Euclidean tensor calculus framework proposed by Arsigny et al.[14] and the affine invariant square root of the J-divergence proposed by Wang and Vemuri.[15] Seed points provided by the user give clues about the location of the object of interest and the background. The locations of the seed points are encoded into the graph providing hard constraints for the segmentation. The user can interactively modify the seed points as needed in order to improve the segmentation results. Using the max-flow algorithm, we efficiently compute the global minimum graph cut guaranteeing an optimal DT-MRI segmentation.

The paper is organized as follows. In section 2.1, we review graph cuts and optimal maximum flow algorithms for computing minimum cuts. In addition, the connection between minimizing energy functions and computation of minimum cut is discussed. Scalar image segmentation using graph cuts is briefly reviewed in section 2.2. In section 2.3, we present our extension of scalar image segmentation using graph cuts to DT-MRI data segmentation. We present experimental segmentation results on both synthetic and real cardiac and brain DT-MRI data in section 3. We summarize and draw concluding remarks in section 4.

2. METHOD

We first present the mathematical background of graph cuts and its use for energy minimization and show the construction of graphs for scalar image segmentation. We then provide the details of our method extending graph cuts to DT-MRI segmentation.

2.1. Graph Cuts Overview

Suppose $G = (V, E)$ is an undirected graph with vertex set V and edge set E. Two special terminal vertices denote the source s and the sink t. An edge in E connecting $u, v \in V$ is assigned a cost $c(u, v)$. An $s - t$ cut $C(S, T)$ partitions V into two disjoint sets S and T, such that $s \in S$ and $t \in T$. The cost of the cut is the sum of all edge costs connecting a vertex in S to a vertex in T:

$$C(S,T) = \sum_{u \in S, v \in T} c(u,v) \tag{1}$$

The minimum $s-t$ cut is the cut C with the smallest cost. Due to the theorem of Ford and Fulkerson,[16] finding the minimum cut is equivalent to computing the maximum flow from the source to the sink, which is solvable in polynomial time.[17]

Since each cut of a graph G has a cost associated with it, we may view the graph G as an energy function mapping from all cuts on G to the set of nonnegative real numbers. Any cut can be described by $|V|$ binary variables $x_1, ..., x_{|V|}$ corresponding to vertices in G (excluding the source and the sink), such that $x_i = 0$ when vertex $v_i \in S$, and $x_i = 1$ when $v_i \in T$. An energy ξ can be represented by G, where ξ is viewed as a function of $|V|$ binary variables $\xi(x_1, ..., x_{|V|})$, and whose value is equal to the cost of the cut defined by the configuration

$x_1, ..., x_{|V|}$ ($x_i \in \{0, 1\}$). Such energy function ξ can be efficiently minimized by computing the minimum cut of G or simply the "graph cut".[18]

The standard form of the energy function can be written as

$$\xi(x_1, ..., x_{|V|}) = \sum_{p \in \{1,2,...,|V|\}} \zeta_p(x_p) \; + \sum_{\substack{p,q \in \{1,2,...,|V|\} \\ v_q \in \mathcal{N}_p, q \neq p}} \zeta_{p,q}(x_p, x_q) \tag{2}$$

where where $\mathcal{N}_p$ is the neighborhood of vertex v_p.

The first term $\zeta_p(x_p)$ measures the cost of assigning a binary value x_p to a vertex v_p, which designates whether v_p belongs to the set S or T after the minimum cut is computed. From a segmentation point of view, this term is derived from the image data and is computed by measuring the similarity between the voxel corresponding to v_p and other known object or background voxels. The second term $\zeta_{p,q}(x_p, x_q)$ measures the cost of assigning x_p and x_q to the adjacent vertices v_p and v_q. Once again, from a segmentation point of view, this cost reflects conformance to boundary properties. The cost function is computed in such a way that similar neighboring image voxels are associated with graph vertices that are connected by higher cost edges, whereas dissimilar voxels are associated with lower cost edges. At the borders of objects, adjacent voxels should have different labels and it is important that the energy function ξ not over penalize such labeling.

2.2. Scalar Image Segmentation Using Graph Cuts

As explained in the previous section, a cut is a binary partition of a graph and can be viewed as a labeling of the graph. Binary segmentation, which is a binary partition of image voxels, can therefore be performed by first creating a graph with vertices corresponding to the image voxels and edges with proper weights, and then employing efficient polynomial time minimum graph cut algorithms.[17] While there are generalizations of the minimum $s - t$ cut problem that involve more than two terminals, such as the multiway cut problem,[19] such generalizations are generally NP-hard.

Boykov and Jolly[13] proposed an interactive technique for segmenting N-dimensional scalar images using graph cuts. In this method the user imposes hard constraints for segmentation by indicating certain pixels (seeds) that absolutely have to be part of the object and certain pixels that have to be part of the background. Intuitively, these hard constraints provide clues on what the user intends to segment. The rest of the image is segmented automatically by constructing a cost function whose minimization results in a globally optimum segmentation among all segmentations satisfying the hard constraints. The cost function is defined in terms of edges that form boundary and region properties. The boundary property ensures that voxels on either side of a boundary are dissimilar while the region property ensures voxels belonging to the same region are similar to each other and dissimilar to voxels (seeds) known to belong to different image partitions.

2.3. Extending Segmentation Using Graph Cuts to DT-MRI Data

In the proposed DT-MRI graph cuts interactive segmentation technique, the user first selects certain tensor voxels belonging to the structure or object to be segmented, henceforth denoted by *"obj"*, and background tensor voxels belonging to the background, henceforth denoted by *"bkg"*. These so called seed tensors constitute hard constraints for the segmentation, i.e., after segmentation *obj* seeds must remain labeled as belonging to the object of interest while *bkg* seeds must remain labeled as background. Since typically more than one solution can satisfy these hard constraints, these conditions are considered insufficient for defining a single optimal segmentation and additional soft constraints are used to automatically label all remaining tensors in the image. The soft constraints are incorporated into the energy function through edge weights, reflecting both boundary and region properties.

2.3.1. Energy Function

Consider an arbitrary N-dimensional tensors field $\mathcal{T}$. Let $A = (A_1, A_2, ...A_{|\mathcal{T}|})$ be a binary vector that defines a segmentation of $\mathcal{T}$, where each element A_i specifies whether tensor T_i belongs to the object or background. This is the same as the binary labeling problem described in section 2.1 for which an energy functional can be constructed and minimized efficiently using graph cuts.

We define an energy functional $\xi(A)$ as[13]

$$\xi(A) = \lambda \cdot R(A) + B(A) \tag{3}$$

where

$$R(A) = \sum_{T_i \in \mathcal{T}} R_{T_i}(A_i), \quad and \tag{4}$$

$$B(A) = \sum_{\substack{i,j \in \{1,2,\ldots,|\mathcal{T}|\} \\ T_j \in \mathcal{N}_i, i \neq j}} B_{(T_i,T_j)} \tag{5}$$

where $\mathcal{N}_i$ is the set of tensors neighboring tensor T_i. The coefficient $\lambda \geq 0$ in (3) specifies a relative importance of region properties term $R(A)$ versus the boundary properties term $B(A)$. The boundary term $B_{(T_i,T_j)}$ is interpreted as the penalty for discontinuity between neighboring tensors (T_i, T_j). Normally $B_{(T_i,T_j)}$ is large when the neighboring tensors are similar and close to zero when they are dissimilar. The regional term $R(A)$ sums up the individual penalties $R_{T_i}(A_i)$ of assigning a tensor T_i as *obj* or *bkg* and is computed by examining the dissimilarity measure of tensor T_i compared to the *obj* and *bkg* seed tensors.

2.3.2. Graph Construction

We now construct a graph G as follows. Each tensor voxel of the DT-MR image corresponds to a non-terminal node in the graph. We add two terminal nodes, namely source s and sink t so that a flow is pushed from s to t (figure 1). Neighboring tensors (T_i, T_j) are connected by edges with edge weights of $B_{(T_i,T_j)}$. In our work we have considered 8-connectivity neighborhood for 2D data and 26-connectivity for 3D data. Moreover, each non-terminal node is connected to the terminal nodes with edge weights given as in table 1.

Table 1. Edge weight assignment table for the graph G

Edge	Weight	For
(T_i, T_j)	$B_{(T_i,T_j)}$	$(T_i, T_j) \in \mathcal{N}, T_j \in \mathcal{N}_i, i \neq j$
(T_i, s)	$\lambda R_{T_i}(bkg)$	$T_i \notin \mathcal{O} \cup \mathcal{B}$
	K	$T_i \in \mathcal{O}$
	0	$T_i \in \mathcal{B}$
(T_i, t)	$\lambda R_{T_i}(obj)$	$T_i \notin \mathcal{O} \cup \mathcal{B}$
	0	$T_i \in \mathcal{O}$
	K	$T_i \in \mathcal{B}$

where

$$K = 1.0 + \max_{T_i \in \mathcal{T}} \sum_{\substack{i,j \in \{1,2,\ldots,|\mathcal{T}|\} \\ T_j \in \mathcal{N}_i, i \neq j}} B_{(T_i,T_j)} \tag{6}$$

and $\mathcal{O}$ and $\mathcal{B}$ denote the set of *obj* and *bkg* seed tensors respectively.

The edge weight of a non-terminal tensor T_i to the source terminal node s is the penalty of assigning the tensor T_i as *bkg* tensor denoted by $R_{T_i}(bkg)$. Similarly, the edge weight of a non-terminal tensor T_i to the sink terminal node t is the penalty of assigning the tensor T_i as *obj* tensor denoted by $R_{T_i}(obj)$.

By assigning the weight K, which is greater than the sum of all edge weights of a seed tensor to its neighbors, to the edges connecting each *obj* and *bkg* seed points to s and t respectively, we ensure that the hard constraints of the segmentation will always remain intact after segmentation. This comes from the fact that the minimum graph cut always severs the least weight edges. Moreover by definition, this cut will sever one and only one terminal link from each tensor; thus resulting in an optimal segmentation. Also note that the region and boundary terms are not yet defined and their definition will rely on tensor dissimilarity metrics detailed in the next section.

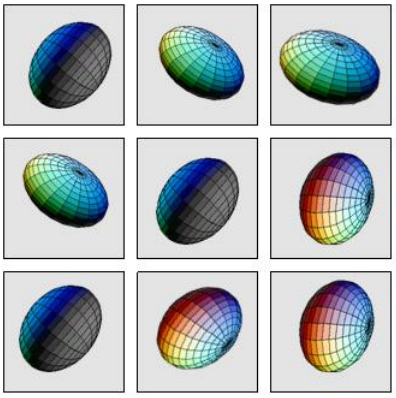

(a) Image before segmentation

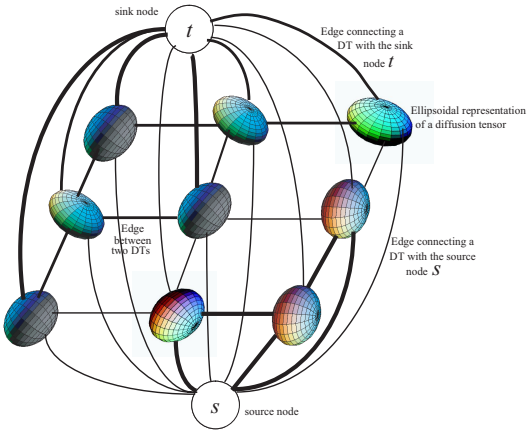

(b) Graph before minimum cut

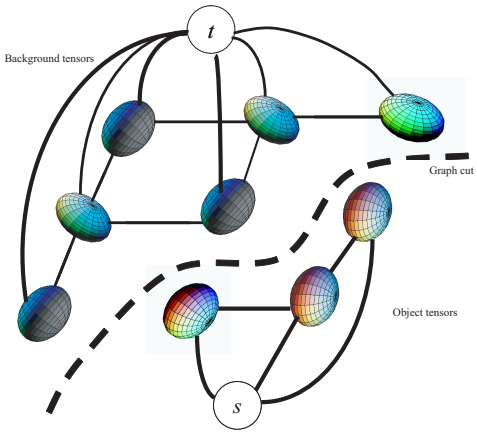

(c) Graph after minimum cut

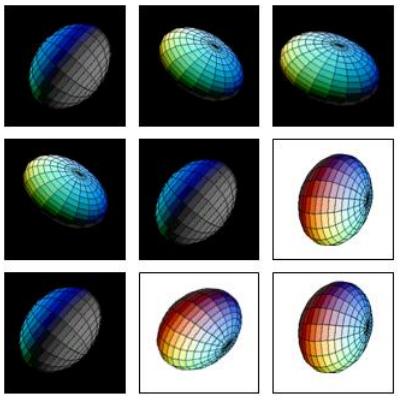

(d) Image after segmentation

Figure 1. Simple illustration of graph construction from 2D 3×3 DT-MR image (a). The cost of each edge is reflected by the edge's thickness (b). Low cost edges are attractive choices for the minimum cut. The cut (c) separates the tensors into object and background classes (d). The 3D ellipsoids are used to visualize diffusion tensors where the directions and lengths of the major axes correspond to the eigenvectors and eigenvalues of the diffusion tensors.

2.3.3. Tensor Dissimilarity Measures

In order to fully utilize all the information in the tensors while computing the edge weights of the graph, the dissimilarity measure of tensors should incorporate both diffusion magnitudes and directions in the DT-MR image. We utilize the Log-Euclidean or the Affine Invariant tensor distance measure for computing these edge weights.[14, 15]

The Log-Euclidean tensor distance, d_{LE}, and the Affine Invariant, d_{AI}, tensor distances between tensors T_i and T_j are computed as in equations 7 and 8 respectively, where $tr(.)$ denotes the trace of a matrix, log is matrix logarithm and n is the size of the tensors T_i and T_j (which is 3 in DT-MR images).

$$d_{LE}(T_i, T_j) = \sqrt{tr((log(T_i) - log(T_j))^2)} \tag{7}$$

$$d_{AI}(T_i, T_j) = \frac{1}{2}\sqrt{tr(T_i^{-1}T_j + T_j^{-1}T_i) - 2n} \tag{8}$$

We compute the boundary link weights $B_{(T_i,T_j)}$ as the inverse of tensor distance between T_i and T_j.

$$B_{(T_i,T_j)} = f(d(T_i, T_j)) \tag{9}$$

where d is either d_{LE} or d_{AI} and f is a monotonically decreasing function that maps the range of tensor-dissimilarity values to the interval (0, 1].

The weights of the terminal links connecting a non-seed tensor to the terminal nodes are obtained by computing the distance of each such tensor from all seed tensors and averaging these distances. Specifically, the edge weight of a non-seed tensor T_i to the source terminal node s, which is the penalty of assigning the tensor T_i as bkg tensor, is given by

$$R_{T_i}(bkg) = \frac{\sum_{T_j \in \mathcal{B}} d(T_i, T_j)}{|\mathcal{B}|} \tag{10}$$

Similarly, the weight of a non-seed tensors T_i to the sink terminal node t, which is the penalty of assigning the tensor T_i as obj tensor, is given by

$$R_{T_i}(obj) = \frac{\sum_{T_j \in \mathcal{O}} d(T_i, T_j)}{|\mathcal{O}|}. \tag{11}$$

3. EXPERIMENTAL RESULTS

In this section, we present some simulation results of the proposed segmentation technique for both synthetic and real data. Both Log Euclidean and Affine Invariant tensor dissimilarity measures were tested and gave similar results.

3.1. Synthetic Data

Figure 2 shows a noisy synthetic DT-MR image segmentation performed with the proposed technique. This example is used to demonstrate that full tensor information must be used to achieve quality segmentation for tensor fields. The inner circle contains anisotropic diffusion with a preferred direction pointing left (in the figure) while the outer circle contains anisotropic diffusion tensors of the same magnitude with preferred direction of diffusion pointing downward. In order to test the strength of our segmentation algorithm, random Gaussian noise was added independently to the three eigenvalues of the DT-MR image[20] in addition to random rotation (in azimuth and elevation) perturbing the three eigenvectors by the same amount to retain orthogonality. Scalar quantities derived from tensors such as fractional an isotropy would not discriminate such image as having distinct diffusion properties. By considering the diffusion direction in addition to the magnitude however, we could correctly interpret the image as having two distinct structures with entirely different diffusion properties and thus segmented the image accordingly.

In figure 3, we show that the proposed method is capable of segmenting an object of interest made up of several disconnected parts.

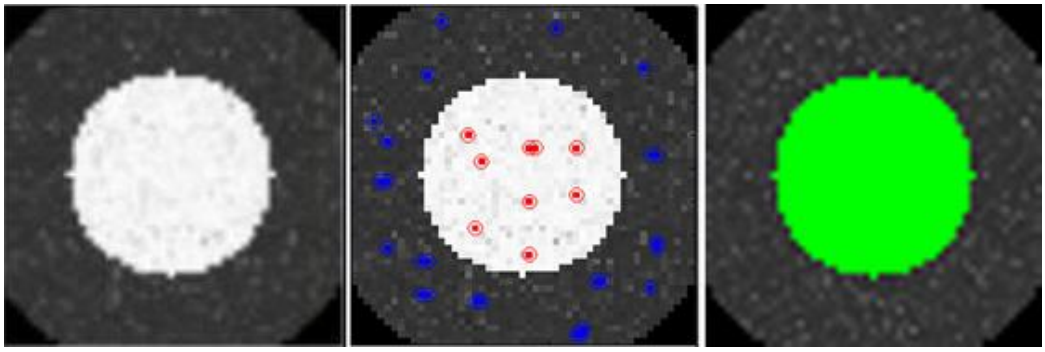

Figure 2. Segmentation of a noisy synthetic 2D DT-MRI slice. (left) The DT-MRI slice visualized using only the scalar first entry of the tensor field $T(1,1)$. The inner 'white' disk contains tensor pixels with eigenvectors $(1,0,0),(0,1,0),(0,0,1)$ and corresponding eigenvalues $(10,1,1)$. The outer disk contains tensors with eigenvectors $(0,1,0),(1,0,0),(0,0,1)$ and corresponding eigenvalues of $(10,1,1)$. Gaussian noise is then used to corrupt the eigenvalues and to rotate the eigenvectors. (middle) Manually selected object seed points (red) and background seed points (blue). (right) Segmentation result shown in green.

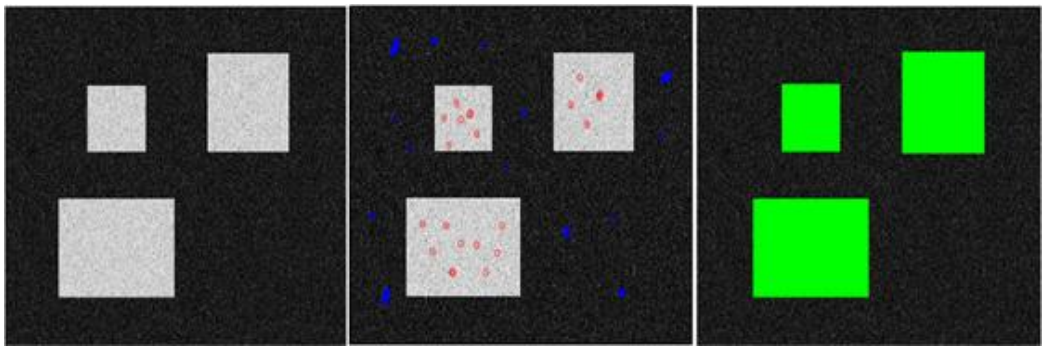

Figure 3. Segmentation of a synthetic noisy DT-MRI slice containing an object comprising several disconnected parts. (left) The DT-MIR slice visualized using $T(1,1)$. (middle) Object (red) and backgrounds (blue) seed points. (right) Segmentation result in green. The tensors inside the object and the tensors forming the background were created in a manner similar to those in figure 2.

3.2. Real Data

While the synthetic example demonstrated the quality of segmentation results obtained by the proposed technique, the practicality of the proposed technique was evaluated using real brain and cardiac DT-MRI data as shown below. Figure 4, shows segmentation result of brain corpus callosum where white matter is segmented out from the remaining part of the brain. No regularization, smoothing or interpolation was performed prior to segmentation. Figure 5 shows the segmentation result for the cardiac ventricles.

4. CONCLUSIONS

We extended graph cuts to segment DT-MR images. We made use of tensor calculus and tensor dissimilarity metrics to define edge weights in the graphs. We applied the results to segmenting real and synthetic DT-MRI data. The method was successful in the experiments we performed. Future work includes more comprehensive quantitative evaluation, comparison to other methods, and speed enhancement. Another future research direction is to investigate DT-MRI visualization techniques that allow the user to view and explore the complete information in the diffusion tensors during the interactive seed placement stage.

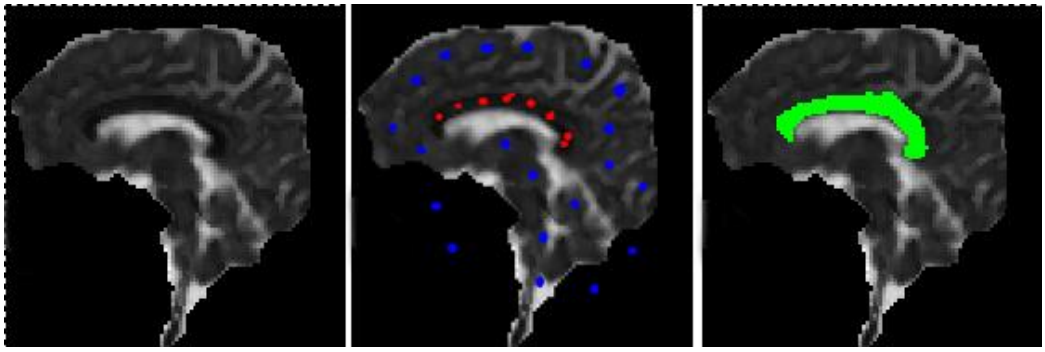

Figure 4. Corpus callosum (CC) segmentation from a DT-MRI slice of the brain. (left) The DT-MRI slice visualized using $T(1,1)$. (middle) Manually selected CC seed points (red) and background seed points (blue). (right) CC segmentation result shown in green.

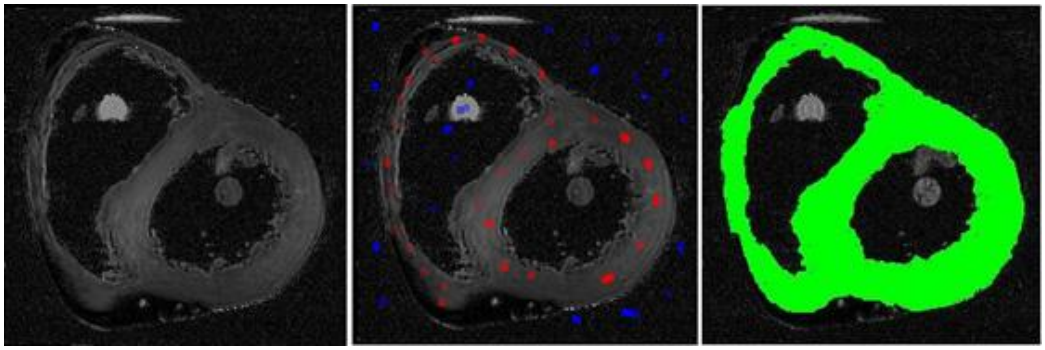

Figure 5. Cardiac wall segmentation from a DT-MRI slice of the heart. (left) The DT-MRI slice visualized using $T(1,1)$. (middle) Manually selected heart seed points (red) and background seed points (blue). (right) Cardiac segmentation result shown in green.

5. ACKNOWLEDGEMENTS

We would like to thank Yuri Boykov and Vladimir Kolmogorov for making their computer program for computing maximum flow available for the public which we used in our work*. Our thanks also goes to Drs. Patrick A. Helm and Raimond L. Winslow at the Center for Cardiovascular Bioinformatics and Modeling, Dr. Elliot McVeigh at the National Institute of Health for provision of the cardiac DT-MRI data† and Dr. Khader Hasan, Department of Diagnostic and Interventional Imaging, University of Texas Medical School at Houston, for provision of the brain DT-MRI data.

REFERENCES

1. P. Basser, J. Mattiello, and D. LeBihan, "Estimation of the effective self-diffusion tensor from the NMR spin echo.," *Journal of Magnetic Resonance B* **103**(3), pp. 247–54, 1994.
2. L. Zhukov, K. Museth, D. Breen, R. Whitaker, and A. Barr, "Level set modeling and segmentation of DT-MRI brain data," *Journal of Electronic Imaging* **12**(1), pp. 125–133, 2003.
3. Z. Wang and B. Vemuri, "DTI segmentation using an information theoretic tensor dissimilarity measure," *Medical Imaging, IEEE Transactions on* **24**(10), pp. 1267–1277, 2005.
4. L. ODonnell, W. Grimson, and C. Westin, "Interface Detection in Diffusion Tensor MRI," *MICCAI 2004 Part 1, Proceedings of* , pp. 360–367, 2004.

*Available at http://www.cs.cornell.edu/People/vnk/software.html
†From http://www.ccbm.jhu.edu/research/DTMRIDS.php

5. A. Brun, H. Knutsson, H. Park, M. Shenton, and C. Westin, "Clustering Fiber Traces Using Normalized Cuts," *MICCAI* , pp. 368–375, 2004.
6. C. Feddern, J. Weickert, and B. Burgeth, "Level-Set Methods for Tensor-Valued Images," *Second IEEE Workshop on Variational, Geometric and Level Set Methods in Computer Vision, Proceedings of* , pp. 65 – 72, 2003.
7. C. Lenglet, R. Deriche, and O. Faugeras, "Inferring white matter geometry from diffusion tensor MRI: Application to connectivity mapping," *ECCV 2004, PT 4, Proceedings of* , pp. 127–140, 2004.
8. C. Lenglet, M. Rousson, and R. Deriche, "Segmentation of 3d probability density fields by surface evolution: Application to diffusion mri," *Proc. 7th Intl. Conf. on Medical Image Computing and Computer Assisted Intervention, Saint-Malo, France, September* , 2004.
9. C. Lenglet, M. Rousson, R. Deriche, O. Faugeras, S. Lehericy, and K. Ugurbil, "A Riemannian Approach to Diffusion Tensor Images Segmentation," *Proceedings of the 19th International Conference on Information Processing in Medical Imaging (IPMI), Glenwood Springs, CO, USA* , pp. 591–602, 2005.
10. M. Rousson, C. Lenglet, and R. Deriche, "Level Set and Region Based Surface Propagation for Diffusion Tensor MRI Segmentation," *CVAMIA and MMBIA* **3**(5), pp. 123–134, 2004.
11. R. Deriche, D. Tschumperle, and C. Lenglet, "DT-MRI estimation, regularization and fiber tractography," *Biomedical Imaging: Macro to Nano, 2004. IEEE International Symposium on* , pp. 9–12, 2004.
12. M. Wiegell, D. Tuch, H. Larsson, and V. Wedeen, "Automatic segmentation of thalamic nuclei from diffusion tensor magnetic resonance imaging," *Neuroimage* **19**(2), pp. 391–401, 2003.
13. Y. Boykov and M. Jolly, "Interactive graph cuts for optimal boundary and region segmentation of objects in ND images," *International Conference on Computer Vision* **1**, pp. 105–112, 2001.
14. V. Arsigny, P. Fillard, X. Pennec, and N. Ayache, "Log-euclidean metrics for fast and simple calculus on diffusion tensors," *Magnetic Resonance in Medicine* **56**, pp. 411–421, 2006.
15. Z. Wang and B. Vemuri, "An affine invariant tensor dissimilarity measure and its applications to tensor-valued image segmentation," *CVPR* **1**, pp. 1267–1277, 2004.
16. L. Ford and D. Fulkerson, "Flow in Networks," *Princeton University Press, Princeton, NJ* , 1962.
17. A. Goldberg and R. Tarjan, "A new approach to the maximum-flow problem," *Journal of the ACM (JACM)* **35**(4), pp. 921–940, 1988.
18. V. Kolmogorov and R. Zabin, "What energy functions can be minimized via graph cuts?," *Pattern Analysis and Machine Intelligence, IEEE Transactions on* **26**(2), pp. 147–159, 2004.
19. E. Dahlhaus, D. Johnson, C. Papadimitriou, P. Seymour, and M. Yannakakis, "The Complexity of Multi-terminal Cuts," *SIAM J. Comput.* **23**(4), pp. 864–894, 1994.
20. M. Welk, C. Feddern, B. Burgeth, and J. Weickert, "Median filtering of tensor-valued images," in *Pattern Recognition*, B. Michaelis and G. Krell, eds., *Lecture Notes in Computer Science* **2781**, pp. 17–24, Springer, Berlin, 2003.